3.C

Nuclear Physics **45** (1963) 492—504; © *North-Holland Publishing Co., Amsterdam*

ELASTIC SCATTERING OF RELATIVISTIC ELECTRONS BY SCREENED ATOMIC NUCLEI

SHIN-R LIN † and NOAH SHERMAN

Physics Department, University of Michigan, Ann Arbor, Michigan

and

JEROME K. PERCUS

Courant Institute of Mathematical Sciences, New York University, New York ††

Received 25 February 1963

Abstract: The effect of screening by atomic electrons on the scattering of relativistic electrons by heavy atoms has been computed numerically using different screening models. Exponential and Hartree potentials were used to simulate the screening. The asymmetry factor $S(\theta)$ and the differential scattering cross section $d\sigma(\theta)/d\Omega$ were computed at 15 degree intervals from 15° to 165°. We report here the results for (a) 121 keV electrons scattered by gold, $Z = 79$, using two exponential potentials of different range, (b) 79 keV ($v/c = 0.5$) electrons scattered by mercury, $Z = 80$, using exponential and Hartree fields, (c) 46 keV ($v/c = 0.4$) electrons scattered by mercury as in (b). The asymmetry factor $S(\theta)$ and $d\sigma/d\Omega(\theta)$ were computed using a partial wave expansion in which the phase shifts were obtained both by numerical integration of a suitably transformed Dirac radial equation and also computed in WKB approximation. The results are compared with corresponding calculations for the Coulomb field. In general the differences are no more than a few percent, but below 30° the screened field cross-sections are as much as 50% smaller.

1. Introduction

One of the methods in current use for measuring the transverse polarization of electron beams with energies below 500 keV is Mott scattering [1, 2]). This method assumes the applicability of the Mott theory [3]) for the single scattering of electrons by heavy atoms, in which the effect of screening by atomic electrons, among other phenomena, is ignored. In this paper we report the results of numerical calculations which attempt to include the screening effect.

The Mott calculations predict that the electrons scattered out of a polarized beam by heavy point nuclei will be distributed with an azimuthal asymmetry about the axis of the incident beam. This asymmetry depends on the transverse polarization of the incident beam, its energy, the scattering angle and the charge of the nucleus. If the asymmetry factor $S(\theta)$ is known at experimentally accessible angles (which constitute the central fraction of the range of angles reported in this paper), the polarization

† Now at Physics Department, Yale University, New Haven, Connecticut.

†† This work was supported in part by the Office of Naval Research, the National Science Foundation and the U. S. Atomic Energy Commission, Contract AT(30-1) 1480 and is based in part on thesis submitted by one of the authors (S.R.L.) in partial fulfillment of the requirements for the Ph. D. degree in Physics at the University of Michigan.

of the beam can be deduced from measurements of the azimuthal distribution of the scattered electrons.

The screening effect has been investigated by Bartlett and Welton [4]) and more recently by Mohr and Tassie [5]). Unfortunately, the errors in their calculations are probably greater than the experimental errors in recent polarization measurements [1, 2]) which are claimed to be accurate to within a few per cent. The computations reported here represent an effort to determine the screening effect as accurately as possible. As screening potentials, we first chose one-term exponential potentials for gold and mercury and then calculations for mercury with Hartree † potentials [6]) were added. The low-l phase shifts are calculated by the numerical integration of differential equations, and the high-l phase shifts are obtained from the WKB approximation. All computations are carried out on IBM-704 and IBM-7090 computers at the University of Michigan and at the AEC Computing Center, New York University.

In the following section, we first discuss the procedure used to obtain phase shifts by the numerical integration of differential equations. Sect. 3 is devoted to the discussion of the results for six different computations. In the final section, we offer our conclusions.

2. Computation of Phase Shifts

2.1. LOW-l PHASE SHIFTS

To obtain the low-l phase shifts, we have to integrate either [3])

$$\begin{aligned} \frac{\mathrm{d}F_l}{\mathrm{d}r} &= -\frac{l+2}{r}F_l+\beta G_l, \\ \frac{-\mathrm{d}G_l}{\mathrm{d}r} &= \alpha F_l-\frac{l}{r}G_l, \end{aligned} \tag{1}$$

where

$$\left.\begin{matrix}\alpha\\ \beta\end{matrix}\right\} = \frac{1}{\hbar c}(E-V\pm mc^2),$$

or

$$\frac{\mathrm{d}^2 g_l}{\mathrm{d}r^2}+\left\{k^2-\frac{l(l+1)}{r^2}-U_l\right\}g_l = 0. \tag{2}$$

Here U_l is the effective Dirac potential

$$U_l = \frac{2E}{\hbar^2c^2}V-\frac{V^2}{\hbar^2c^2}-\frac{l+1}{r}\frac{\alpha'}{\alpha}+\tfrac{3}{4}\frac{\alpha'^2}{\alpha^2}-\tfrac{1}{2}\frac{\alpha''}{\alpha}.$$

The phase shift δ_l is defined in such a way that the asymptotic forms of g_l and G_l are proportional to $\sin(kr-\frac{1}{2}l\pi+\delta_l)$. The functions g_l and G_l are regular at the origin.

† We are indebted to Dr. Martin J. Berger of the National Bureau of Standards for informing one of the authors (S.R.L.) of the existence of the numerical data on the Hartree field for mercury.

Similarly δ_{-l-1} is a phase shift with l replaced by $-(l+1)$ in the asymptotic solutions of eqs. (1) and (2). When we try to integrate eqs. (1) or (2) numerically using the Runge-Kutta integration scheme, the Adams method or the predictor-corrector scheme, we find that these procedures are either extremely time-consuming or the solution becomes unstable after the long-range integration. We, therefore, introduce convenient transformations to facilitate the numerical integrations. In the following we describe two transformations that we use in the computations.

2.1.1. *First transformation*

To integrate eq. (2), we introduce the transformation

$$g_l(\xi) = A_l(\xi)\sin(\xi+\eta_l(\xi)), \qquad \xi = kr. \tag{3}$$

After the differentiation, we have

$$\frac{dg_l}{d\xi} = \frac{dA_l}{d\xi}\sin(\xi+\eta_l)+A_l\cos(\xi+\eta_l)+\frac{d\eta_l}{d\xi}A_l\cos(\xi+\eta_l). \tag{4}$$

Since we can choose either $A_l(\xi)$ or $\eta_l(\xi)$ arbitrarily, we impose the condition

$$\frac{dA_l}{d\xi}\sin(\xi+\eta_l)+\frac{d\eta_l}{d\xi}A_l\cos(\xi+\eta_l) = 0. \tag{5}$$

Then eq. (4) reduces to

$$\frac{dg_l}{d\xi} = A_l\cos(\xi+\eta_l). \tag{4}$$

Using eqs. (2), (4)′ and (5), we have two equations:

$$\frac{1}{A_l}\frac{dA_l}{d\xi} = \left[\frac{l(l+1)}{\xi^2}+\frac{U_l}{k^2}\right]\sin(\xi+\eta_l)\cos(\xi+\eta_l), \tag{6}$$

$$\frac{d\eta_l}{d\xi} = -\left[\frac{l(l+1)}{\xi^2}+\frac{U_l}{k^2}\right]\sin^2(\xi+\eta_l). \tag{7}$$

The properties of $A_l(\xi)$ and η_l as $r\to\infty$ are

$$\eta_l \underset{r\to\infty}{\to} \delta_l-\tfrac{1}{2}l\pi, \qquad A_l \underset{r\to\infty}{\to} \text{constant}.$$

Since eq. (2) has the same form as the radial part of the non-relativistic Schrödinger equation, we can use formally identical methods to obtain the phase shifts. We recall that in the Schrödinger theory these quantities can be determined from the ratio $(1/g_l)dg_l/d\xi$ where the latter quantity is evaluated at some point ξ_0 in a region where $V(r)$ is negligible for all $r \geqq r_0$. In a similar way the ratio of $(1/g_l)dg_l/d\xi$ in the region where U_l is negligible compared with other terms is all we need for the determination

of phase shifts in the relativistic treatment. Thus we have to integrate eq. (7) alone. It turns out that eq. (7) can be integrated efficiently by the Runge-Kutta [8, 9]) fifth-order numerical procedure. The necessary initial values of η_l are obtained from the power series expansions of η_l and U_l in terms of ξ near the origin, with the condition that g_l be regular there.

2.1.2. *Second transformation*

To integrate eq. (1), we introduce the transformation [10])

$$G_l = A_l(r)\frac{\cos\phi_l(r)}{r}, \qquad F_l = A_l(r)\frac{\sin\phi_l(r)}{r}, \tag{8}$$

then after substitution into eq. (1) and some manipulations, we get

$$\frac{1}{A_l}\frac{\mathrm{d}A_l}{\mathrm{d}r} = \frac{l+1}{r}\cos 2\phi_l - \frac{mc^2}{\hbar c}\sin^2\phi_l, \tag{9}$$

$$\frac{\mathrm{d}\phi_l}{\mathrm{d}r} = -\frac{l+1}{r}\sin 2\phi_l + \frac{1}{\hbar c}(E-V) - \frac{mc^2}{\hbar c}\cos 2\phi_l. \tag{10}$$

Again, as in subsect. 2.1.1. we can show that to determine phase shifts, we need the ratio $(1/G_l)\mathrm{d}G_l/\mathrm{d}r$, which from eqs. (1) and (8) is

$$\frac{G_l'}{G_l} = -\alpha\frac{F_l}{G_l} + \frac{l}{r} = -\alpha\,\mathrm{tg}\,\phi_l + \frac{l}{r}$$

at points $r \geqq a$ where $V(a) \approx 0$ compared with E. Thus we can integrate eq. (10) instead of eq. (1). The initial value of ϕ_l is obtained by the expansion of ϕ_l in a power series in r near the origin with the condition that G_l be regular at the origin. Eq. (10) is again integrated by the Runge-Kutta fifth-order method. In practice the combination of the two transformations is found to be the least time-consuming method. Therefore we use this combination in computing most of the phase shifts for small l.

In actual calculation, a further change of variable for small r was introduced. Following Hartree [7]), we set

$$Y = \ln\xi = \ln ka_{\mathrm{B}}X.$$

We used this transformation in the region $r < 1a_{\mathrm{B}}$. In this region $0 < X < 1$ where $X = r/a_{\mathrm{B}}$, the intervals (0, 1) in X-axis corresponds to the interval $(-\infty, 0)$ in Y-axis. The integration step size is then $\Delta Y = \Delta X/X$, and the advantage of this transformation lies in the fact that a constant step size ΔY corresponds to a varying

step size in ΔX in X-axis. Thus the necessity of changing step sizes in X-axis as X increases was taken care of automatically.

2.2. HIGH-l PHASE SHIFTS

For high-l phase shifts, the WKB approximation developed by Good [11]) is used. In table 1, we list the phase shifts computed by the method of subsection 2.1 and the WKB approximation for gold at $T = 121$ keV.

TABLE 1

Comparison of phase shifts by different methods

	$Z = 79$		$T = 121$ keV			
	Methods					
	subsect. 2.1.1		subsect. 2.1.2		WKB approx.	
l	δ_l	δ_{-l-1}	δ_l	δ_{-l-1}	δ_l	δ_{-l-1}
0	4.29475		4.29477		4.24460	
1	3.25030	3.61141	3.25072	3.61186	3.23199	3.56269
5	1.93856	1.98080	1.93839	1.98067	1.93632	1.97680
10	1.32039	1.33880	1.32030	1.33868	1.31890	1.33716
20	0.74803	0.75552	0.74781	0.75534	0.74787	0.75503
30	0.46728	0.47130	0.46738	0.47142	0.46728	0.47132
40	0.30491	0.30736	0.30486	0.30728	0.30525	0.30763
50	0.20376	0.20527	0.20435	0.20590	0.20452	0.20600
60	0.13914	0.14018	0.13918	0.14021	0.13988	0.14082
70	0.09582	0.09648	0.09604	0.09670	0.09651	0.09711
80	0.06664	0.06470	0.06685	0.06728	0.06663	0.06735
90	0.04674	0.04705	0.04682	0.04715	0.04677	0.04706
100	0.03305	0.03327	0.03296	0.03317	0.03305	0.03338

Phase-shifts are given in radians.

As can be seen from table 1, the WKB phase shifts begin to be in good agreement with those obtained from the numerical integration of the differential equations for values of l as low as $l \geqq 10$.

We estimate that the errors in the phase shifts may reach $\pm$ 0.001 r, but about 80% of the phase shifts have smaller errors (on the average, the error is $\pm$ 0.0007 r).

3. Results

The quantities we are interested in are the differential cross section $d\sigma/d\Omega$ for the single-scattering of unpolarized electrons and the asymmetry factor $S(\theta)$. These

quantities are defined as

$$\frac{d\sigma}{d\Omega} = |f(\theta)|^2 + |g(\theta)|^2, \tag{11}$$

$$S(\theta) = \frac{i(fg^* - gf^*)}{\frac{d\sigma}{d\Omega}}, \tag{12}$$

where

$$f(\theta) = \frac{1}{2ik}\sum_l [(l+1)\{\exp(2i\delta_l) - 1\} + l\{\exp(2i\delta_{-l-1}) - 1\}]P_l(\cos\theta), \tag{13}$$

$$g(\theta) = \frac{1}{2ik}\sum_l [\exp(2i\delta_{-l-1}) - \exp(2i\delta_l)]P_l^1(\cos\theta). \tag{14}$$

Eqs. (13) and (14) were summed until the variation in $S(\theta)$ due to the last thirty terms was less than 1 %. The polynomials P_l and P_l^1 are generated from the recursion relations. The accuracy of our summation has been tested in several ways, which will be discussed in sect. 4.

We compute $d\sigma/d\Omega$ and $S(\theta)$ for the following scatterers, potentials and kinetic energies:

a) gold $V = -79e^2 \exp(-3r/a_B)/r$ $T = 121$ keV,

b) gold $V = -79e^2 \exp(-6r/a_B)/r$ $T = 121$ keV,

c) mercury $V = -80e^2 \exp(-3r/a_B)/r$ $\beta = \frac{v}{c} = 0.5$ ($T = 79$ keV),

d) mercury $V = -80e^2 \exp(-3r/a_B)/r$ $\beta = \frac{v}{c} = 0.4$ ($T = 46$ keV),

e) mercury Hartree potential [6]) $\beta = \frac{v}{c} = 0.5$,

f) mercury Hartree potential [6]) $\beta = \frac{v}{c} = 0.4$.

We want to remark here that in the last two cases, in which the Hartree potentials are given in tabulated form, all necessary values not listed were obtained by interpolation. Moreover, the necessary values of derivatives of these potentials were obtained numerically.

In the following, we discuss each case separately.

a) $V = -79\ e^2 \exp(-3r/a_B)/r$, $T = 121$ keV This is the most interesting case in our series of computations. We can compare our results with Sherman's [12]) computation for the Coulomb field, the screened-field results of Mohr and Tassie [5]) and the

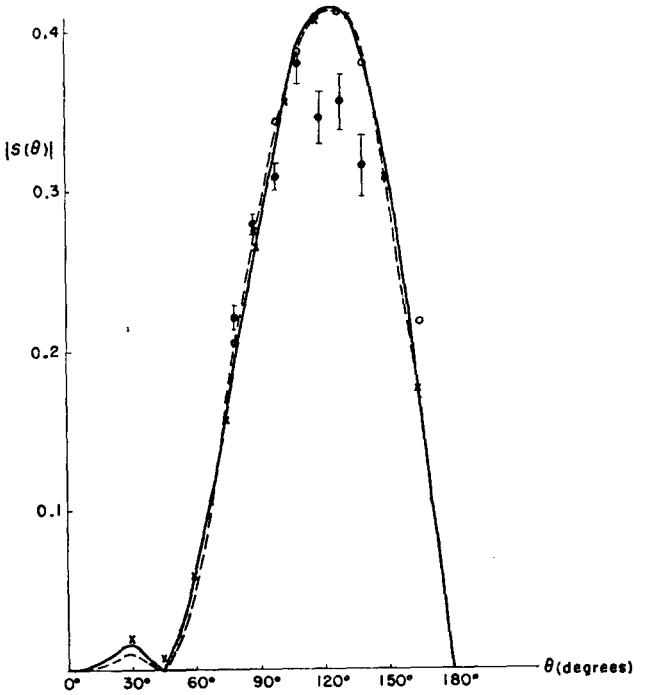

Fig. 1. The asymmetry factor $|S(\theta)|$ for gold at $T = 121$ keV. The full line represents Sherman's results, the dashed line is calculated for $r_0 = \frac{1}{3} a_B$; × $r_0 = \frac{1}{6} r_B$, ○ Mohr and Tassie, ● Nelson and Pidd (exp.).

TABLE 2

Values of the asymmetry factor for gold at $T = 121$ keV

θ (degrees)	Sherman	screened $r_0 = \frac{1}{3} a_B$	Nelson and Pidd (exp.)	screened $r_0 = \frac{1}{6} a_B$
15	$3.347 \cdot 10^{-3}$	$3.2670 \cdot 10^{-3}$		$4.6000 \cdot 10^{-3}$
30	$1.616 \cdot 10^{-2}$	$1.1467 \cdot 10^{-2}$		$1.9415 \cdot 10^{-2}$
45	$1.446 \cdot 10^{-3}$	$2.2434 \cdot 10^{-3}$		$4.9585 \cdot 10^{-3}$
60	$-6.133 \cdot 10^{-2}$	$-5.4420 \cdot 10^{-2}$		$-5.9035 \cdot 10^{-2}$
75	$-1.586 \cdot 10^{-1}$	$-1.6962 \cdot 10^{-1}$		$-1.5595 \cdot 10^{-1}$
			-0.219 ± 0.008 (80°)	
90	$-2.666 \cdot 10^{-1}$	$-2.7118 \cdot 10^{-1}$	-0.274 ± 0.008 (90°)	$-2.6285 \cdot 10^{-1}$
			-0.307 ± 0.008 (100°)	
105	$-3.601 \cdot 10^{-1}$	$-3.6350 \cdot 10^{-1}$		$-3.5491 \cdot 10^{-1}$
			-0.378 ± 0.012 (110°)	
120	$-4.136 \cdot 10^{-1}$	$-4.1036 \cdot 10^{-1}$	-0.344 ± 0.015 (120°)	$-4.0800 \cdot 10^{-1}$
			-0.354 ± 0.015 (130°)	
135	$-4.058 \cdot 10^{-1}$	$-4.0555 \cdot 10^{-1}$		$-4.0925 \cdot 10^{-1}$
			-0.314 ± 0.019 (140°)	
150	$-3.264 \cdot 10^{-1}$	$-3.3101 \cdot 10^{-1}$		$-3.0864 \cdot 10^{-1}$
165	$-1.824 \cdot 10^{-1}$	$-1.8140 \cdot 10^{-1}$		$-1.7426 \cdot 10^{-1}$

measurements of $S(\theta)$ by Nelson and Pidd [13]). We calculated the phase shifts up to $l = 109$ by numerical integration of the differential equations and for $110 \leqq l \leqq 300$ by the WKB approximation. We plot all the results † in fig. 1 for comparison and list them in table 2. At this energy, from 90° and up, the screening effect seems to be small (less than 3%). Our results agree within 2% with the results of Mohr and Tassie except at 165° where our $S(165°)$ is much closer to the value for the Coulomb field. Our results agree with the measured values of Nelson Pidd up to 110°, but above that angle the disagreement is large (more than 15%). (Nelson and Pidd attribute the difference between their values and Sherman's to the plural and multiple scatterings of electrons in the target during the measurements.)

TABLE 3

Differential cross section for gold at $T = 121$ keV

θ (degrees)	Sherman	screened $r_0 = \frac{1}{3} a_B$	screened $r_0 = \frac{1}{6} a_B$
15	$2.349 \cdot 10^6$	$2.0188 \cdot 10^6$	$1.5190 \cdot 10^6$
30	$1.600 \cdot 10^5$	$1.5516 \cdot 10^5$	$1.3945 \cdot 10^5$
45	$3.790 \cdot 10^4$	$3.7397 \cdot 10^4$	$3.6456 \cdot 10^4$
60	$1.494 \cdot 10^4$	$1.5000 \cdot 10^4$	$1.4940 \cdot 10^4$
75	$7.591 \cdot 10^3$	$7.6475 \cdot 10^3$	$7.5763 \cdot 10^3$
90	$4.482 \cdot 10^3$	$4.6578 \cdot 10^3$	$4.7876 \cdot 10^3$
105	$2.936 \cdot 10^3$	$3.0513 \cdot 10^3$	$3.1668 \cdot 10^3$
120	$2.093 \cdot 10^3$	$2.1524 \cdot 10^3$	$2.2227 \cdot 10^3$
135	$1.612 \cdot 10^3$	$1.6918 \cdot 10^3$	$1.6870 \cdot 10^3$
150	$1.336 \cdot 10^3$	$1.3945 \cdot 10^3$	$1.5160 \cdot 10^3$
165	$1.194 \cdot 10^3$	$1.1868 \cdot 10^3$	$1.3740 \cdot 10^3$

Cross section is given in barns per steradian.

As for the differential cross section, at smaller angles the screened field gives smaller values than the pure Coulomb field as expected, but for 60° and up, the differential cross-sections for the screened potential are larger than those for the Coulomb field (see table 3).

b) $V = -79\ e^2\ \exp(-6r/a_B)/r$, $T = 121$ keV. The only difference between this case and case a) is that the screening constant r_0 here is $\frac{1}{6}a_B$ as compared with $r_0 = \frac{1}{3}a_B$ in case a). We computed phase shifts up to $l = 30$ by numerical integration of the differential equations and for $l = 31$ and up, we used the WKB approximation. From fig. 1 and table 1, we can see that this change in r_0 does not result in any drastic change in $S(\theta)$. As for the differential cross section, the deviations from the values for the pure Coulomb field are larger than in case a).

† We remark here that since we plot $|S(\theta)|$ in fig. 1, the cusp near 45° is due to the change of sign in $S(\theta)$ in the neighbourhood of 45°.

c) $V = -80\ e^2 \exp(-3r/a_B)/r$, $\beta = 0.5$. Here we calculated phase shifts up to $l = 40$ by numerical integration of the differential equations and from $l = 41$ to $l = 175$ by the WKB approximation. The screening effect is most prominent in this case. At 120° and 135°, where the measurements are usually carried out, the screening effect in $S(\theta)$ is as much as 15% and this should easily be observed experimentally. As for the differential cross section, the derivation from the values of the pure Coulomb field is again most evident at 15°.

TABLE 4

Asymmetry factors for $Z = 80$

	$\beta = \frac{v}{c} = 0.5$			$\beta = \frac{v}{c} = 0.4$		
θ (degrees)	Coulomb	$V = \frac{Ze^{-\frac{3r}{a_B}}}{r}$	Hartree	Coulomb	$V = \frac{Ze^{-\frac{3r}{a_B}}}{r}$	Hartree
15	$1.60 \cdot 10^{-3}$	$1.66 \cdot 10^{-3}$	$2.98 \cdot 10^{-3}$	$-4.25 \cdot 10^{-4}$	$-7.39 \cdot 10^{-4}$	$-6.65 \cdot 10^{-5}$
30	$1.96 \cdot 10^{-2}$	$2.34 \cdot 10^{-2}$	$2.39 \cdot 10^{-2}$	$1.53 \cdot 10^{-2}$	$1.62 \cdot 10^{-2}$	$2.12 \cdot 10^{-2}$
45	$2.01 \cdot 10^{-2}$	$2.45 \cdot 10^{-2}$	$2.48 \cdot 10^{-2}$	$3.93 \cdot 10^{-2}$	$4.59 \cdot 10^{-2}$	$4.82 \cdot 10^{-2}$
60	$-3.80 \cdot 10^{-2}$	$-3.37 \cdot 10^{-2}$	$-3.23 \cdot 10^{-2}$	$2.18 \cdot 10^{-2}$	$1.42 \cdot 10^{-2}$	$1.42 \cdot 10^{-2}$
75	$-1.43 \cdot 10^{-1}$	$-1.36 \cdot 10^{-1}$	$-1.42 \cdot 10^{-1}$	$-1.04 \cdot 10^{-1}$	$-9.22 \cdot 10^{-2}$	$-9.42 \cdot 10^{-2}$
90	$-2.61 \cdot 10^{-1}$	$-2.56 \cdot 10^{-1}$	$-2.61 \cdot 10^{-1}$	$-2.34 \cdot 10^{-1}$	$-2.23 \cdot 10^{-1}$	$-2.29 \cdot 10^{-1}$
105	$-3.56 \cdot 10^{-1}$	$-3.50 \cdot 10^{-1}$	$-3.60 \cdot 10^{-1}$	$-3.33 \cdot 10^{-1}$	$-3.27 \cdot 10^{-1}$	$-3.27 \cdot 10^{-1}$
120	$-4.01 \cdot 10^{-1}$	$-3.59 \cdot 10^{-1}$	$-3.83 \cdot 10^{-1}$	$-3.72 \cdot 10^{-1}$	$-3.63 \cdot 10^{-1}$	$-3.56 \cdot 10^{-1}$
135	$-3.80 \cdot 10^{-1}$	$-3.29 \cdot 10^{-1}$	$-3.60 \cdot 10^{-1}$	$-3.42 \cdot 10^{-1}$	$-3.34 \cdot 10^{-1}$	$-3.25 \cdot 10^{-1}$
150	$-2.95 \cdot 10^{-1}$	$-2.86 \cdot 10^{-1}$	$-2.74 \cdot 10^{-1}$	$-2.52 \cdot 10^{-1}$	$-2.43 \cdot 10^{-1}$	$-2.36 \cdot 10^{-1}$
165	$-1.61 \cdot 10^{-1}$	$-1.18 \cdot 10^{-1}$	$-1.43 \cdot 10^{-1}$	$-1.37 \cdot 10^{-1}$	$-1.03 \cdot 10^{-1}$	$-1.24 \cdot 10^{-1}$

Cross section for $Z = 80$

	$\beta = \frac{v}{c} = 0.5$			$\beta = \frac{v}{c} = 0.4$		
θ (degrees)	Coulomb	$V = \frac{Ze^{-\frac{3r}{a_B}}}{r}$	Hartree	Coulomb	$V = \frac{Ze^{-\frac{3r}{a_B}}}{r}$	Hartree
15	$5.35 \cdot 10^{6}$	$3.96 \cdot 10^{6}$	$2.80 \cdot 10^{6}$	$1.47 \cdot 10^{7}$	$8.51 \cdot 10^{6}$	$5.86 \cdot 10^{6}$
30	$3.48 \cdot 10^{5}$	$3.22 \cdot 10^{5}$	$2.55 \cdot 10^{5}$	$9.30 \cdot 10^{5}$	$7.83 \cdot 10^{5}$	$5.59 \cdot 10^{5}$
45	$7.93 \cdot 10^{4}$	$7.79 \cdot 10^{4}$	$6.64 \cdot 10^{4}$	$1.99 \cdot 10^{5}$	$1.88 \cdot 10^{5}$	$1.50 \cdot 10^{5}$
60	$3.09 \cdot 10^{4}$	$3.13 \cdot 10^{4}$	$2.80 \cdot 10^{4}$	$7.45 \cdot 10^{4}$	$7.43 \cdot 10^{4}$	$6.24 \cdot 10^{4}$
75	$1.59 \cdot 10^{4}$	$1.62 \cdot 10^{4}$	$1.52 \cdot 10^{4}$	$3.81 \cdot 10^{4}$	$3.89 \cdot 10^{4}$	$3.50 \cdot 10^{4}$
90	$9.64 \cdot 10^{3}$	$9.97 \cdot 10^{3}$	$9.54 \cdot 10^{3}$	$2.35 \cdot 10^{4}$	$2.46 \cdot 10^{4}$	$2.28 \cdot 10^{4}$
105	$6.56 \cdot 10^{3}$	$6.73 \cdot 10^{3}$	$6.64 \cdot 10^{3}$	$1.66 \cdot 10^{4}$	$1.75 \cdot 10^{4}$	$1.75 \cdot 10^{4}$
120	$4.89 \cdot 10^{3}$	$5.21 \cdot 10^{3}$	$5.19 \cdot 10^{3}$	$1.29 \cdot 10^{4}$	$1.41 \cdot 10^{4}$	$1.41 \cdot 10^{4}$
135	$3.95 \cdot 10^{3}$	$4.34 \cdot 10^{3}$	$4.36 \cdot 10^{3}$	$1.10 \cdot 10^{4}$	$1.23 \cdot 10^{4}$	$1.21 \cdot 10^{4}$
150	$3.42 \cdot 10^{3}$	$3.60 \cdot 10^{3}$	$3.80 \cdot 10^{3}$	$9.86 \cdot 10^{3}$	$1.12 \cdot 10^{4}$	$1.16 \cdot 10^{4}$
165	$3.15 \cdot 10^{3}$	$3.04 \cdot 10^{3}$	$3.70 \cdot 10^{3}$	$9.31 \cdot 10^{3}$	$1.06 \cdot 10^{4}$	$1.13 \cdot 10^{4}$

Cross section is given in barns per steradian

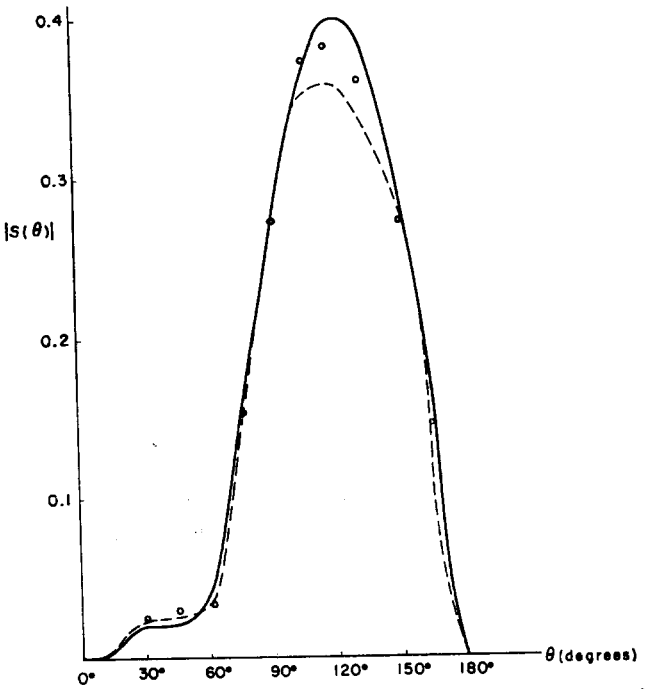

Fig. 2. The asymmetry factor $|S(\theta)|$ for mercury at $T = 79$ keV. Full line: Sherman's results, dashed line: screened results, ⊙ Hartree.

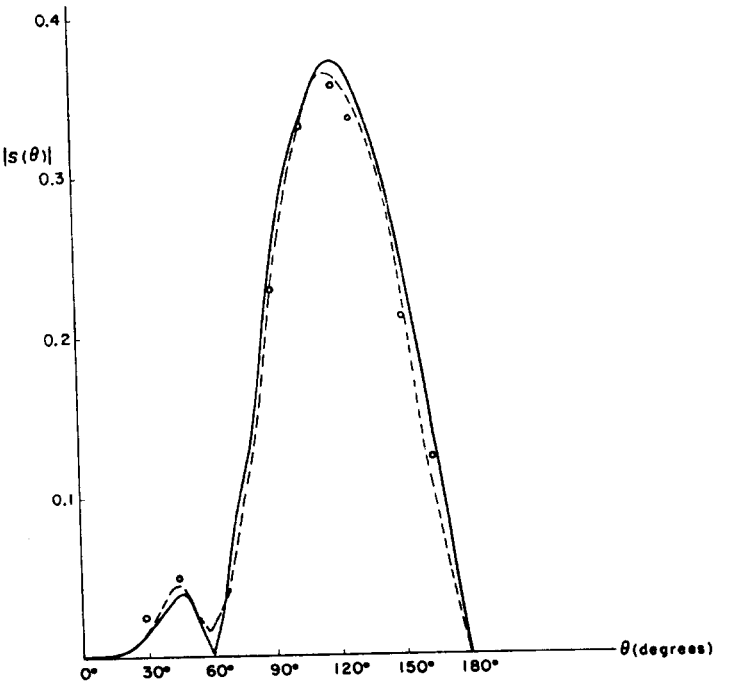

Fig. 3. The asymmetry factor $|S(\theta)|$ for mercury at $T = 46$ keV. See caption to fig. 2.

d) $V = -80\,e^2 \exp(-3r/a_B)/r$, $\beta = 0.4$. The only difference between this case and case c) is that the electron energy here is lower. We might expect that the screening effect in $S(\theta)$ would be more prominent in this case, but this expectation is not confirmed by our results. Instead, $S(\theta)$ is now rather close to the Coulomb $S(\theta)$. The difference is less than 7% in the region 90° to 150°. As for the differential cross section, the deviation from the Coulomb case is very large (as much as 50%). This is much larger than the corresponding difference in case c).

e) Hartree Potential, $\beta = 0.5$. This calculation was made to see whether the large screening effects in $S(\theta)$ seen in case c) is a general characteristic of screened fields. Phase shifts were calculated up† to $l = 100$ by numerical integration of the differential equation and from $l = 101$ to 300, the WKB approximation was used. It turns out that with this potential, the screening effect in $S(\theta)$ is much smaller than in c) at large angles. It never exceeds 6% at large angles (in comparison with c), where it may reach 15%). As for the differential cross section, $d\sigma(\theta)/d\Omega$ for the Hartree field at $\theta < 105°$ is smaller than those of the Coulomb and exponential fields, but above $\theta = 135°$, the Hartree field gives the largest cross section.

f) Hartree Potential, $\beta = 0.4$. This is the repetition of case d). Phase shifts were calculated up to $l = 250$. The WKB approximation was used for $l > 100$. We expected that the screening would be more prominent than in case e), but we did not find this to be the case. The screening effect in $S(\theta)$ is less than 6% at large angles. As for the cross sections, the Hartree field gives the smaller values up to $\theta = 90°$ then becomes larger at $\theta > 150°$.

4. Discussion of Errors and Conclusions

The maximum error in a phase shift is estimated to be less than ± 0.001 rad. The series (13) and (14) are summed with the usual computer precision (8 significant figures) up to the terms where the variation in $S(\theta)$ contributed by the last thirty terms is less than 1%. To check this summation method, we made the following tests:

a) For two cases, the series (13) and (14) are summed using double precision (16 digit numbers). The $P_l(\cos\theta)$ and $P_l^1(\cos\theta)$ polynomials were also generated from the recursion relation by the double precision method. Comparison of the resulting S and $d\sigma/d\Omega$ for all angles with those S and $d\sigma/d\Omega$ which are calculated by single precision, showed that they agree to at least three significant figures in S and four significant figures in $d\sigma/d\Omega$.

b) In summing series of this type, there might be a large relative error, if the large neighbouring terms cancel each other strongly, leaving a small, less accurate residual. To test this possibility, we separate the summation into two parts, each with the same

† Since the Hartree potential decreases much more slowly than the exponential potential as r increases, more phase shifts are needed here than in case c).

sign, adding positive and negative terms separately. At the end, the difference of the two parts is taken and S and $d\sigma/d\Omega$ are calculated. The resulting S and $d\sigma/d\Omega$ agree with the previously calculated S and $d\sigma/d\Omega$ to at least four significant figures, showing that cancellation errors are negligible.

c) To test the round off error in the summation process, we calculate the series

$$\sum_{l=0}^{300}(2l+1)e^{-al}P_l(\cos\theta)$$

for $a = 0.05$ and 0.1 and compare them with the analytically summed results. It is found that they agree to at least four significant figures in both cases.

Finally, to estimate errors in S and $d\sigma/d\Omega$, we added and subtracted an artificial error ε in the phase shifts (1) systematically and (2) randomly. The reason for introducing ε was to determine how sensitively the angular distributions of S and $d\sigma/d\Omega$ depend on errors in the phase shifts. If artificial errors in δ_l give rise to $S(\theta)$ and $d\sigma(\theta)/d\Omega$ which are in erratic disagreement with the original values, we have a fair idea of the accuracy of δ_l and δ_{-l-1} implied by the original smooth distribution.

For $\varepsilon = 0.0001$ introduced at random in δ_l and δ_{-l-1}, $S(\theta)$ showed deviations of as much as 20%. We would infer from these rough tests that the random errors in our (unaltered) phase shifts are not appreciably larger than those that would distort the smooth behaviour of $S(\theta)$ and $d\sigma(\theta)/d\Omega$. These tests, together with estimates of round-off errors, lead us to estimates for S and $d\sigma/d\Omega$ as follows: the error in $S(\theta)$ is $\leqq 3\%$ for $60° \leqq \theta \leqq 150°$ and 9% in $15° \leqq \theta \leqq 45°$ and at 165°. The error in $d\sigma/d\Omega$ is estimated to be less than 3% at all angles. We should point out that in the interval from 15° to 60°, $S(\theta)$ is very small so that the errors in the phase shifts produce larger relative errors in $S(\theta)$.

We would like to express our gratitude to Robert T. Brown, R. H. Bartels and T. Aronstein for their assistance in the computation. We are indebted to the staff of the computing Center at the University of Michigan and to Dr. M. Goldstein and the staff of the AEC Computing Center, Courant Institute of Mathematical Sciences, New York University, for their generous help in the course of calculation.

References

1) J. S. Greenberg, D. P. Malone, R. L. Gluckstern and V. W. Hughes, Phys. Rev. **120** (1960) 1393
2) P. E. Spivak, L. A. M. Kaelian, L. E. Kutikov and V. F. Apalin, JETP (Soviet Physics) **12** (1961) 127
3) N. F. Mott and H. S. W. Massey, The theory of atomic collisions (Oxford U. Press, Oxford, 1949) second ed., pp. 74-85
4) J. H. Bartlett and T. A. Welton, Phys. Rev. **59** (1941) 281
5) C. B. O. Mohr and L. J. Tassie, Proc. Phys. Soc. **A67** (1954) 711
6) S. Cohen, The Rand Corporation, RM-2272-AEC, 1958
7) D. R. Hartree, The calculation of atomic structures (John Wiley and Sons, New York, 1957) p. 99

8) W. Kutta, Z. Math. Phys. **46** (1901) 435
9) E. J. Nystrom, Acta Soc. Sci. Fennicae **50** (1926) 56
10) M. E. Rose, Phys. Rev. **82** (1951) 470
11) R. H. Good, Jr., Phys. Rev. **90** (1953) 131
12) N. Sherman and D. F. Nelson, Phys. Rev. **114** (1959) 1541
13) D. F. Nelson and R. W. Pidd, Phys. Rev. **114** (1959) 728
14) N. Sherman, Phys. Rev. **103** (1956) 1601
15) Yennie Ravenhall and Wilson, Phys. Rev. **95** (1955) 500